Methodology and Calculator for High Precision Regression Fits of Pyranometer Angular Responsivities and the Associated Uncertainties[1]

Matthew Boyd

National Institute of Standards and Technology (NIST), Gaithersburg, Maryland, USA

Abstract

An easy to implement method for accurately utilizing pyranometer incidence angle dependent calibration factors, or responsivities ($\mu V/W/m^2$), along with the associated uncertainties has been developed. This method uses algorithms for creating single polynomial functions dependent on the incidence angle to characterize both the pyranometer responsivity and the upper prediction interval of the associated standard uncertainties. Single polynomial functions are easier to implement in spreadsheet software and programming environments than the simpler to formulate piecewise polynomials and splines. The polynomials are of high degree, extrapolated to 0° and 90°, and solved using robust techniques to avoid oscillations and overshoots, which can occur when using other interpolation methods. A free software tool was created that calculates the functions using the algorithms presented in this paper, and it was tested on the calibrated responsivities and uncertainties of 40 pyranometers representing six (6) different models. All of the obtained fits closely represent the data with R^2 values greater than 0.98.

Keywords: Pyranometer; Responsivity; Incidence Angle; Uncertainty

1. Introduction

The default method of converting pyranometer signals to engineering units, as suggested by pyranometer manufacturers and prevalent in the solar resource community, is to divide the pyranometer output signal in micro-volts (μV) by a constant responsivity in $\mu V/W/m^2$ to obtain the shortwave irradiance in W/m^2. This approach does not account for the large incidence angle (angle from the surface normal) dependency of the responsivity, nor to a lesser extent the effect of net infrared radiation ($net\ IR = IR_{in} - IR_{out}$). Responsivities can vary 5 % from the middle of a 0° to 70° incidence angle range and cause equally large differences in the measured irradiance. These differences, or errors, can have large impacts on a range of applications, one being solar photovoltaics (PV) where power output is proportional to the irradiance. It has been suggested that a 1 % increase in a PV project's yield results in a 10 % increase in the project's profitability (Granata and Howard, 2011), so even small improvements in the irradiance measurements can have a large impact on PV's viability and bankability.

Methods to correct for the incidence angle and net-IR response of pyranometers have been published (Myers et al., 2002; Reda et al., 2008), but adoption has been slow due to the more extensive calibration procedure needed to obtain incidence angle dependent responsivities, as well as the added complexity of applying the calibrated responsivities and uncertainties. The National Renewable Energy Laboratory (NREL) offers the only known calibration service that provides the incidence angle dependent responsivities, termed the Broadband Outdoor Radiometer Calibration (BORCAL) (Reda et al., 2008), but as customary with calibration services they do not provide an assessment of how the results may be employed.

The responsivity as a function of incidence angle can be modeled using piecewise polynomial regression, like those used by Reda, Myers, & Stoffel (2008), but the complex regression functions needed for the fit are not easily transferrable to other software and do not include extrapolations beyond the measured range, most importantly to a 0° incidence angle. Single polynomial regression functions are much simpler to implement, but direct solutions using least squares methods like that derived by Reda (1998) can result in overshoots and oscillations between measured data points; they also do not include extrapolations outside the measured range. Lester (2006) presents functions based on the cosine of the incidence angle for modeling the responsivity, but the simple four-term functions do not closely follow the complex responsivity curve or include extrapolations outside the measured range. Furthermore, the stepwise regressions needed to create these individualized functions rely on data measured over a significant time period which is not feasible for most calibrations.

[1] Boyd, M., 2015. Methodology and calculator for high precision regression fits of pyranometer angular responsivities and the associated uncertainties. Solar Energy 119, 233–242. doi:10.1016/j.solener.2015.06.048

Nomenclature

AM	morning
BORCAL	Broadband Outdoor Radiometer Calibration
c_i	polynomial coefficient of the *i*th degree
G	total irradiance, W/m^2
G_{bn}	beam (direct) normal radiation, W/m^2
G_d	diffuse horizontal irradiance, W/m^2
GUM	*Guide to the Expression of Uncertainty in Measurement*
IR	infrared radiation, W/m^2
N_{df}	number of degrees of freedom
NIST	National Institute of Standards and Technology
NREL	National Renewable Energy Laboratory
PM	afternoon
PV	photovoltaic
R	shortwave responsivity, μV/W/m^2
R^2	coefficient of determination
R_{net}	net-IR responsivity, μV/W/m^2
RSS	root-sum-square
SER	standard error of regression
U_{95}	expanded uncertainty at a 95 % confidence level
u_c	combined standard uncertainty
V	voltage, μV
W_{net}	net infrared radiation, W/m^2
x_i	*i*th measured or reference data value
y_i	*i*th modeled or measured data value

Greek symbols

θ	incidence angle, °

Subscripts

bn	beam normal
c	combined
d	diffuse
df	degrees of freedom
i	data point index or polynomial degree
net	input minus output

This paper presents an algorithm for creating single polynomial regression fits of pyranometer responsivities as a function of incidence angle that include extrapolations outside the measured range to 0° and 90°. This paper is not aiming to understand or model the perceived angular response, nor evaluate the validity of the calibration data or calibration service. These calculated functions are interpolations of the calibrated responsivities for easier implementation, not pyranometer calibration curves. They should only be used for similar conditions as those during the calibration, namely for times when the majority of the irradiance is beam (direct) irradiance and thus coming largely from the same incidence angle. The regression functions can be made for either a full range of azimuth (compass direction) angles (i.e., 90° incidence angle in the morning to near 0° at solar noon to 90° incidence angle in the afternoon) or irrespective of azimuth (i.e., 0° to 90°). A second algorithm is also presented for creating single, simple polynomial regression functions of the uncertainty of the responsivity as a function of incidence angle. These two algorithms are employed in a freely distributable software tool that allows easy implementation of the functions for data measured in a BORCAL or similar procedure. This software is then used to test calibration data from six (6) different models of pyranometers.

2. Responsivity Regression

2.1. Measurements

Calibration procedures for indirectly measuring the incidence angle dependent pyranometer responsivities include those by Myers et al. (2002), Reda (2008), and ASTM G167 – 05 (2010). These methods can capture the incidence angle response of the pyranometer during the calibration period and correct for the net-IR response by using the following functional relationship:

$$R(\theta) = \frac{V - W_{net} R_{net}}{G_{bn} \cos(\theta) + G_d} \tag{1}$$

where $R(\theta)$ is the (shortwave) responsivity of the pyranometer corresponding to the incidence angle, V is the voltage signal from the pyranometer, W_{net} is the net-IR radiation measured using a pyrgeometer, R_{net} is the net-IR (longwave) responsivity of the pyranometer, G_{bn} is the beam normal radiation, θ is the incidence angle, and G_d is the horizontal diffuse irradiance. Incidence angles are angles from the normal of the surface, which include pyranometer sensors, while zenith angles are angles between the vertical and a line to the sun; these values are therefore equal for horizontally deployed sensors.

The net-IR responsivity is zero for pyranometers with silicon or black and white thermopile sensors and can range from about (0.1 to 0.7) μV/W/m^2 (Michalsky et al.,2005) for pyranometers with all black thermopile sensors. The net-IR responsivity is typically assumed constant for a given pyranometer model and is provided with calibrations that correct for net-IR. The governing equation of the pyranometer irradiance using these known parameters and calibrated responsivities is:

$$G = \frac{V - W_{net} R_{net}}{R(\theta)} \tag{2}$$

For outdoor calibrations spanning a limited timeframe and in a single location, there is a narrow range of incidence angles for each azimuth angle. Therefore, the responsivities can be binned by azimuth angle into morning ($R_{AM}(\theta)$) and afternoon ($R_{PM}(\theta)$)

sets, and further simplified by denoting negative incidence angles for the morning and positive incidence angles for the afternoon. These angles are relative to the orientation of the pyranometer, which, along with the environmental conditions, must be the same as when calibrated to accurately transfer the calculated responsivities. The orientation includes the azimuth of the pyranometer, indicated by the direction of the connector, and the tilt, which should also be replicated if feasible. The environmental conditions during calibrations are typically chosen to be clear, stable skies, but there are still changing, unaccounted conditions like the irradiance spectrum, temperature of the instrument, and the azimuth and zenith angle combinations of the incident irradiance that may affect the resultant calibrated responsivities, especially if calibrations only span a single day like in the case of BORCALs.

Differences in the AM and PM calibrated responsivities at the same incidence angle may be systematic and a true azimuth response, due to a non-horizontal sensor caused by a misaligned or defective bubble level, or just from uncontrolled or unaccounted factors like changing environmental conditions. Using separate morning and afternoon responsivities can result in higher, systematic errors unbounded by the respective uncertainties than when using the combined responsivities if the differences in the morning and afternoon values are from uncontrolled factors. The separate responsivities are also an incomplete map of the hemispherical azimuth/zenith surface domain of responsivities, which may have more complex variations. Lastly, a major drawback of using these separate responsivities is that there is a discontinuity at solar noon, minus the one or two days of the year when the incidence angle at solar noon is the same as that of the day of the calibration. The discontinuity arises from the AM and PM responsivities meeting at solar noon at a different incidence angle than that during the calibration, where the calibrated values may not be equal.

2.2. Algorithm

The morning (AM) and afternoon (PM) calibrated responsivities can either be averaged together, like shown in Fig. 1, to encapsulate some of the uncertainties arising from the differences in the pyranometer orientation, solar azimuth, and solar spectrum relative to the calibration setup and conditions, or kept separate when the calibration conditions are confidently duplicated. When kept separate, the AM incidence angles are made negative to differentiate them from the PM values, although true incidence angles are only valid between 0° (normal to the receiver surface) and 90°.

The responsivities for the full incidence angle domain are interpolated with respect to the cosine of the incidence angle for the averaged responsivities, or the incidence angle minus 90° for the separate responsivities. This is performed to make the domain unique across the AM and PM values (the cosine of the range -90° to 90° is 0 to 0, while the cosine of the range -180° to 0° is -1 to 1.) Since the data do not follow a simple smooth function, the interpolation is performed using a piecewise cubic Hermite polynomial (Fritsch and Carlson, 1980; Kahaner et al., 1988). This piecewise polynomial makes only the first derivative between subfunction 'pieces' equal, effectively simplifying the connection requirements of the pieces, so there are no

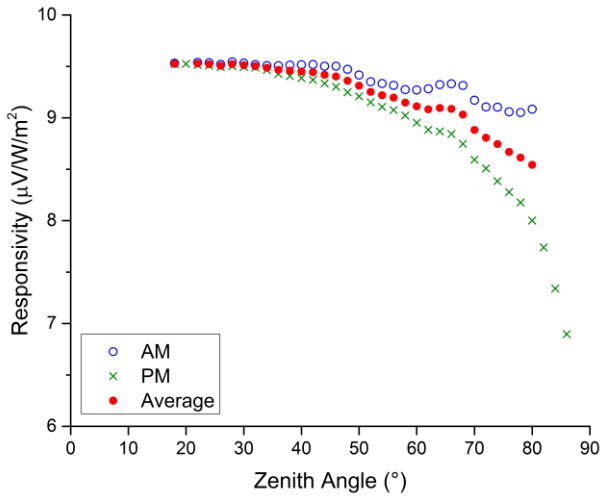

Fig. 1. The morning (AM), afternoon (PM), and averages of the morning and afternoon calibrated responsivities for a pyranometer with a strong azimuth angle response.

overshoots and fewer oscillations between points than other functions like splines that are continuous to higher derivatives between subintervals (more stringent connection requirements.)

The resulting regression function can substantially depart from the anticipated responsivities beyond both the low and high ends of the measurement domain, so two separate extrapolations are performed to 0 (90°) and 1 (0°) for the averaged responsivities, as shown in Fig. 2, and to -1 (-90°) and 1 (90°) for the separate responsivities. These extrapolations are either first or second degree polynomials, depending on the curvature of the interpolation at the boundaries of the domain, and are continuous to the same derivative as the subfunction order at the domain boundaries.

The extrapolations, which are continuous functions valid over the measurement domains, are merged together by first dividing them into a large number of data points (600) following a uniform distribution in incidence angles (°). This distribution is

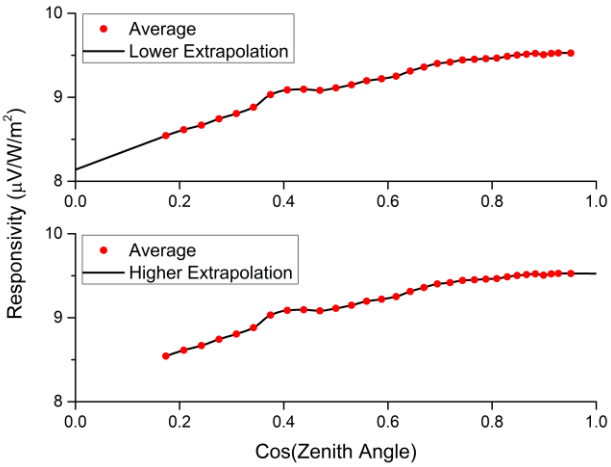

Fig. 2. The polynomial regression fits of the averaged calibrated responsivities including extrapolations to the low and high ends of the measurement domains.

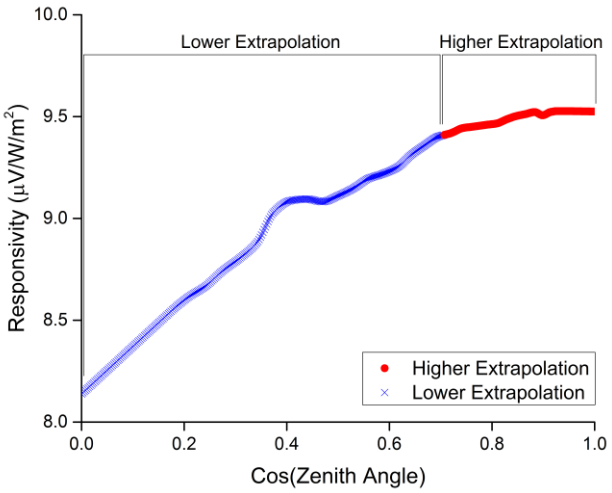

Fig. 3. The merged higher and lower responsivity regression extrapolations.

the same as the data measured in BORCALs (every 2°), and it weights the data more around the cosine of 0° than the cosine of 90° (and -90°), thereby providing a better fit near the lower incidence angles where the uncertainties in the measurements are lower. The two now discrete domains are cropped and joined together at the middle of the measurement domain, near 45° (0.707) for the averaged responsivities, as shown in Fig. 3, or near 0° for the separate responsivities.

A single high-degree polynomial is fit to these values using the following regression functions for the averaged and separate responsivities, respectively:

$$R_{averaged}(\theta) = \sum_{i=0}^{degree} c_i \cdot \cos^i(\theta) \quad (3)$$

$$R_{separate}(\theta) = \sum_{i=0}^{degree} c_i \cdot \cos^i(\theta - 90°) \quad (4)$$

where $R(\theta)$ is the responsivity of the pyranometer as a function of the incidence angle, θ is the incidence angle, *degree* is the degree of the polynomial, i is the degree of the polynomial term, and c_i is the coefficient of the ith degree of the polynomial term. The coefficients for these polynomials are determined by solving $\boldsymbol{Vp} = \boldsymbol{y}$ using the least squares method, where $\boldsymbol{V}$ is the Vandermonde matrix of powers of the regressor (cosine of the incidence angle), $\boldsymbol{p}$ is the vector of polynomial coefficients, and $\boldsymbol{y}$ is the vector of responses (responsivities). Fig. 4 shows the fitted polynomial regression functions and the coefficient of determination (R^2) values for the averaged and separate responsivities for a pyranometer with a strong azimuth angle response, indicated by the non-overlapping AM and PM curves in the plot of the averaged responsivities. This strong azimuth response may be systematic, potentially due to a non-horizontal sensor, sometimes caused by a misaligned or defective bubble level, or effectively a random error from changing environmental conditions. Table 1 gives the coefficients for these polynomial functions in equations (3) and (4), respectively. (Note that the calibration data in this paper are from

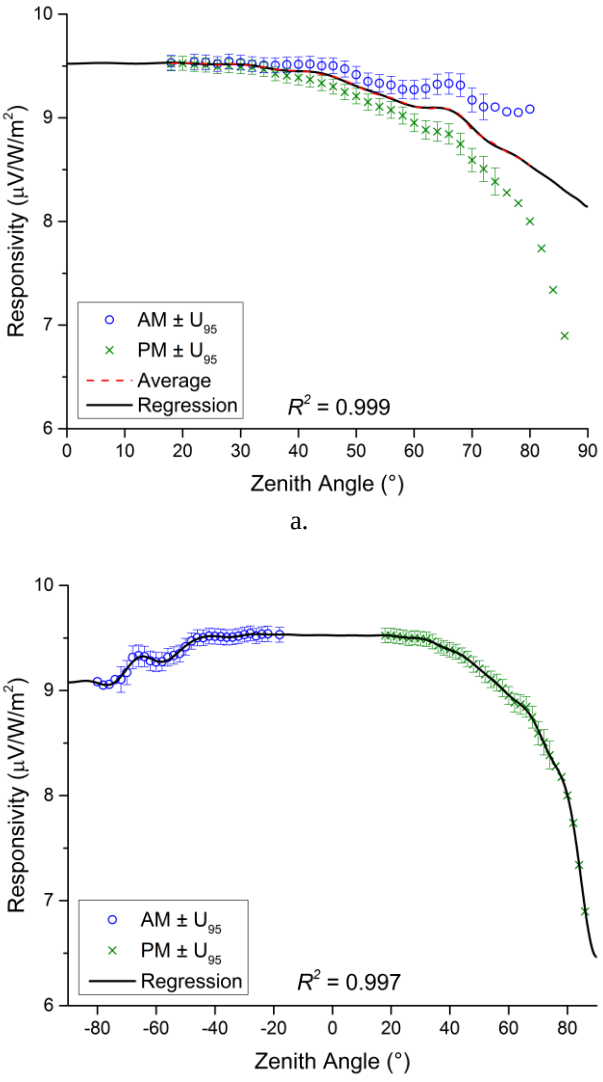

Fig. 4. The polynomial regression fits of the (a.) averaged calibrated responsivities (top) and the (b.) separate morning (AM) and afternoon (PM) calibrated responsivities (bottom) for a pyranometer with a strong azimuth angle response.

pyranometers at a 0° tilt, when the zenith angle equals the incidence angle.)

Very close fitting polynomials that accurately reproduce all of the calibrated values, like those shown in Fig. 4, have a degree of around 20 for the averaged responsivities (about 30 data points) and around 30 for the separate AM and PM responsivities (about 65 data points); however, reasonably good fitting polynomials of only a few degrees can also be found. The coefficients for these polynomials are truncated to 15 digits of precision before plotting to verify that the polynomial will accurately reproduce in software adhering to the IEEE 754 standard for floating-point arithmetic (IEEE, 2008).

Table 1
Polynomial coefficients for the averaged and separate responsivity regression functions in Fig. 4 corresponding to equations (3) and (4), respectively.

Degree	Averaged	Separate
0	8.14465621843780	9.52408507768209
1	-0.985275350835612	-0.0478494148636936
2	333.852679367634	0.269634256789717
3	-13791.9416032383	5.96457220528897
4	298098.155745273	-27.2207758199144
5	-3768672.75046539	-297.471814653980
6	28923184.7363728	983.562679604880
7	-126109037.275420	6850.38284108647
8	151469918.111252	-16767.2757262571
9	1779899390.70525	-87732.4839926921
10	-13725741904.3637	161786.330779906
11	54512629861.3594	690859.475433737
12	-145707054374.137	-977909.209161214
13	281305777686.185	-3568489.23033039
14	-402110446349.740	3922959.55788457
15	427354291898.920	12599007.9111928
16	-334004148014.221	-10795344.7443700
17	186692847347.401	-31142939.7725341
18	-70685198404.3809	20692097.6450205
19	16249356515.4652	54414374.8102810
20	-1713013683.71969	-27604335.0648448
21		-66891688.7415818
22		25137814.3478772
23		56589237.9962269
24		-14902020.6811834
25		-31360062.1405462
26		5183205.87405710
27		10247549.5284177
28		-802445.145958149
29		-1496677.48657719

3. Uncertainty Regression

3.1. Calculation of Standard Uncertainties

The uncertainties of the responsivity values estimated by the regression are calculated in accordance with the *Guide to the Expression of Uncertainty in Measurement* (*GUM*) (JCGM/WG 1, 2010). The Type A (statistical) uncertainties include just the interpolation error calculated using the standard error of the regression (SER):

$$u = \sqrt{\frac{1}{N_{df}} \sum_i \left(y_i - x_i \right)^2} \tag{5}$$

where u is the standard uncertainty, N_{df} is the number of degrees of freedom, which is the number of data points minus the number of fitted parameters, y_i is the ith fitted value, and x_i is the ith data point. For the responsivity regression functions, the number of fitted parameters is the degree of the polynomial plus one, y_i is the responsivity estimated by the regression model at the ith incidence angle, and x_i is the measured responsivity at the ith incidence angle.

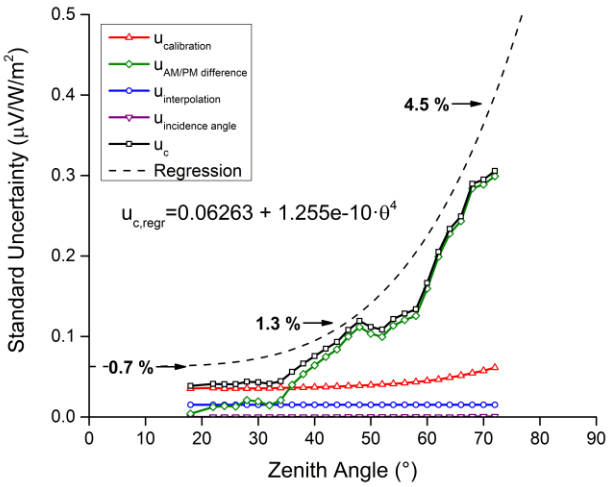

a.

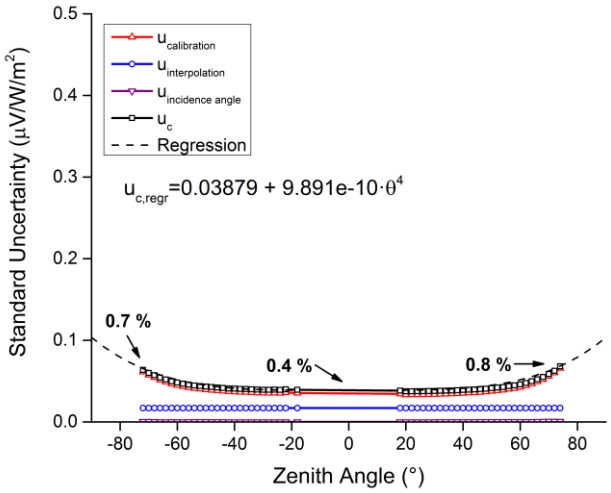

b.

Fig. 5. The polynomial regression fits of the upper bound of the uncertainties for the (a.) averaged calibrated responsivities (top) and the (b.) separate morning (AM) and afternoon (PM) calibrated responsivities (bottom) for a pyranometer with a strong azimuth angle response.

The Type B (non-statistical) uncertainties include those of the calibrated responsivities as propagated from the uncertainties in the measured variables in the responsivity calibration equation (equation (1)), the differences between the AM and PM responsivities, if they are averaged, and the uncertainty in the incidence angle argument to the regression function. The uncertainties in the calibrated responsivities are given in the calibration report or calculated according to a procedure similar to that by Myers et al. (2002), and taken as the maximum of the AM and PM uncertainty if the responsivities are averaged. An unqualified uncertainty from a calibration report is conservatively assumed to be the bounds of a rectangular distribution and is divided by the square root of three to convert it to a standard uncertainty (Taylor and Kuyatt, 2004). The standard uncertainty from the difference in the AM and PM responsivities is calculated as half the difference between the

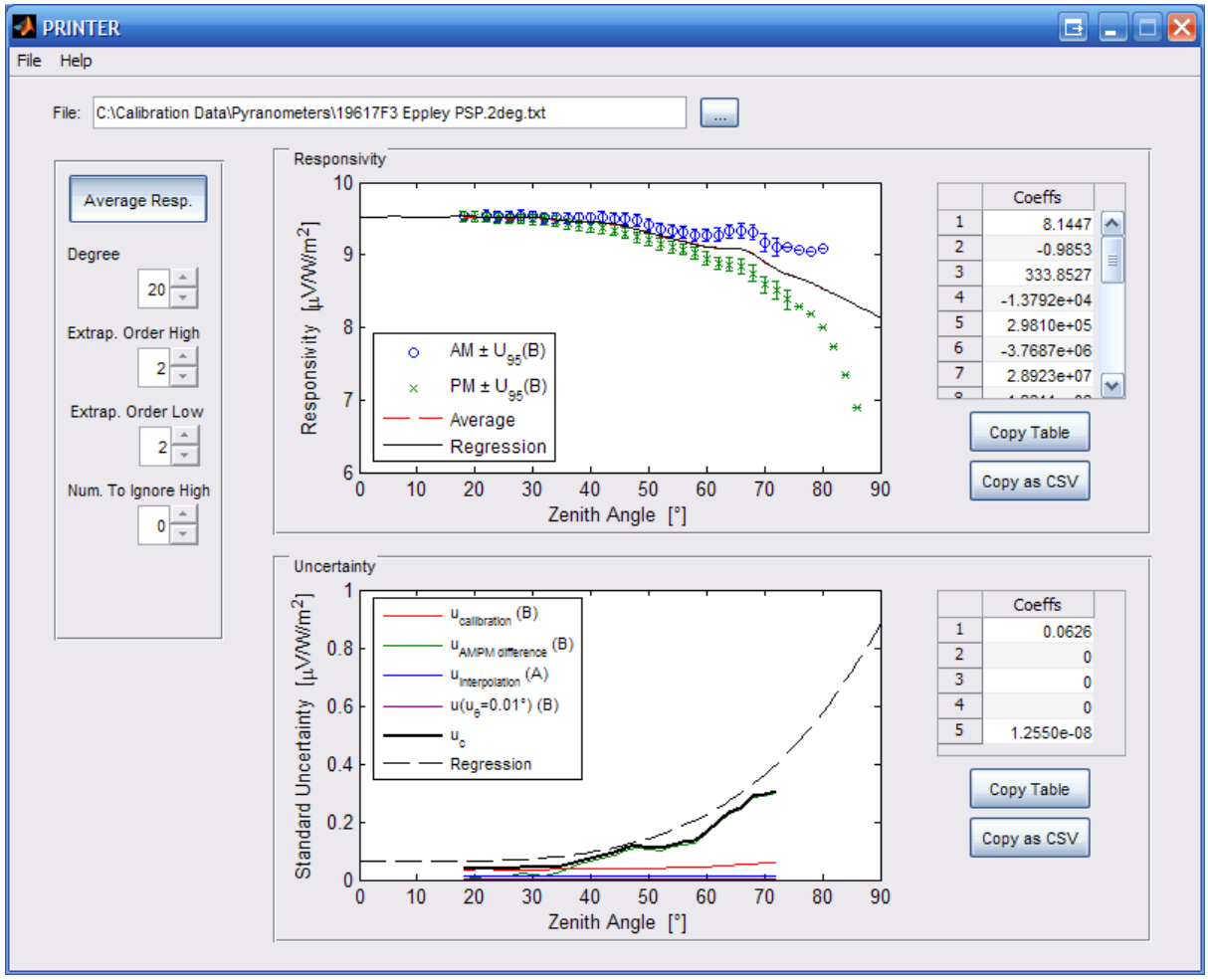

Fig. 6. Screenshot of software tool for calculating pyranometer responsivity and uncertainty regressions (MATLAB, 2010)

values, based on the assumption that there is a 2 in 3 chance that the true responsivity is between the AM and PM values (JCGM/WG 1, 2010).

The standard Type B uncertainty as propagated from the uncertainty in the incidence angle argument to the responsivity regression function is calculated by differentiating this polynomial function with respect to the cosine of the incidence angle, and applying the Chain Rule to get the derivative with respect to the incidence angle:

$$\frac{dR}{d\theta} = \frac{dR}{dz} \cdot \frac{dz}{d\theta} \tag{6}$$

where $z = \cos(\theta)$ and $dz/d\theta = -\sin(\theta)$ for the averaged responsivities and $z = \cos(\theta - 90°)$ and $dz/d\theta = -\sin(\theta - 90°)$ for the separate responsivities, R is the responsivity, and θ is the incidence angle. The resulting propagated uncertainty from multiplying this derivative by the uncertainty in the incidence angle is shown to be negligible for moderately accurate solar position algorithms (Michalsky, 1988; Meeus, 1998) with an uncertainty of ±0.02°, and even for less accurate estimates approaching ±0.5°.

3.2. Algorithm

The root-sum-square (RSS) combinations of these Type A and Type B uncertainties are fit to a nonlinear regression model of the form:

$$u_c = c_0 + c_1\theta^4 \tag{7}$$

using the Levenberg-Marquardt algorithm (Seber and Wild, 2003), where u_c is the combined uncertainty, c_0 is the offset coefficient, c_1 is the scaling coefficient, and θ is the incidence angle. This polynomial has a simple form, zero slope at the 0° incidence angle, and approximates the shape of the combined uncertainties in the 0° to 70° range for the sampling of pyranometers that were evaluated. The resulting polynomial regression function is a 'best-fit', so a six sigma (99.9999999 %) prediction interval is calculated (Lane and DuMouchel, 1994). A second nonlinear regression using the same model and fitting

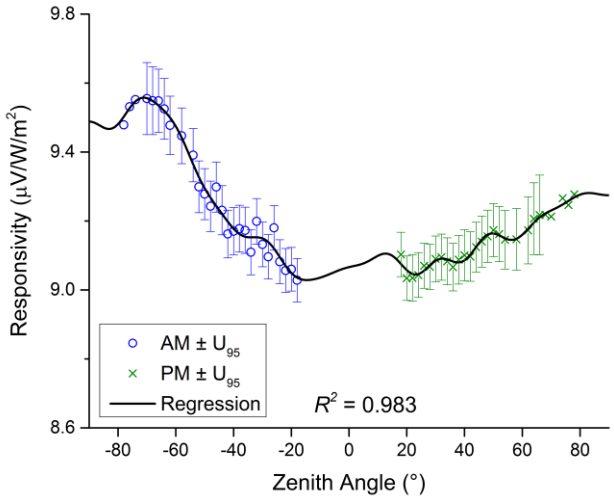

a.

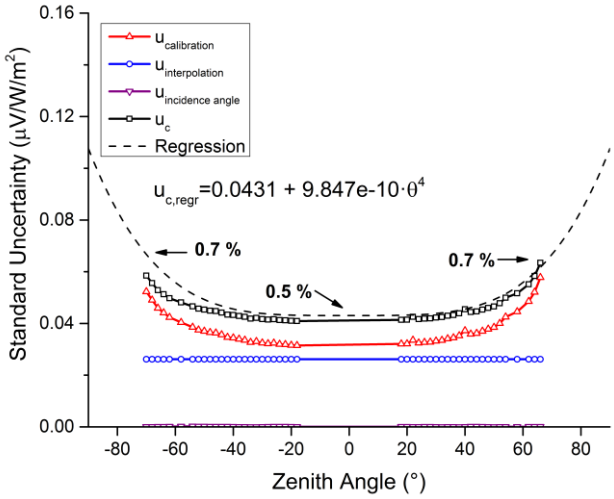

b.

Fig. 7. (a.) The polynomial regression fits of the separate morning (AM) and afternoon (PM) responsivities and (b.) the upper bound of the combined uncertainties for a black-and-white pyranometer, using program parameters: (24,1,1,0,0).

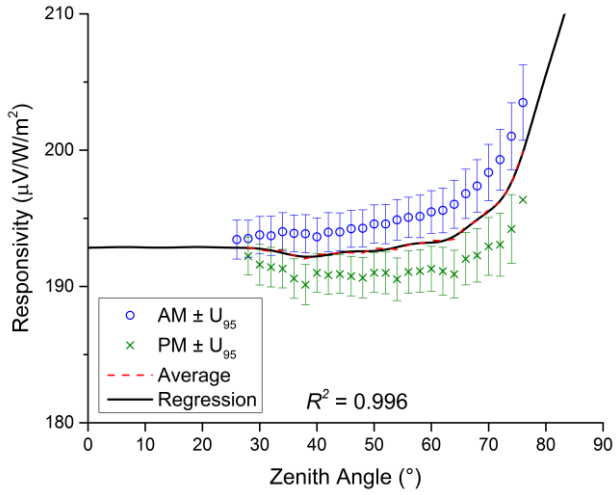

a.

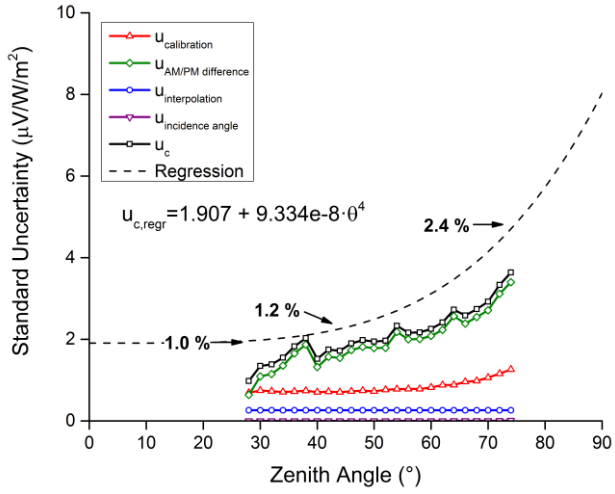

b.

Fig. 8. (a.) The polynomial regression fits of the averaged morning (AM) and afternoon (PM) responsivities and (b.) the upper bound of the combined uncertainties for a domed diffused silicon-cell pyranometer, using program parameters: (19,2,1,0).

algorithm is performed on the upper bound of this prediction interval to ensure that nearly all uncertainties are not underestimated, with the tradeoff that nearly all will be overestimated. Fig. 5 shows the polynomial fitted to the upper bound of the uncertainties for the averaged and separate responsivities for the same pyranometer in Fig. 4 that has a strong azimuth angle response.

4. Software Tool

A software program was created that implements the algorithms in this paper, with a screenshot shown in Fig. 6. This tool can be freely downloaded from the NIST webserver at http://www.nist.gov/el/building_environment/heattrans/ and includes the source code and separate spreadsheet and coding templates for implementing the regressions. Either NREL BORCAL or similarly formatted input data files can be selected through the tool's graphic user interface along with:

- the option to average the AM and PM responsivities or keep them separate (default = average)
- the degree of the polynomial responsivity regression (default = 19 for averaged, 29 for separate)
- the degree of each polynomial extrapolation (default = 2)
- the number of data points to ignore from the high incidence angle ends of the data set (default = 0)

After processing, separate plots of the responsivity and uncertainty regression fits overlaid on the input data are shown on the main screen. Also given are the polynomial coefficients in ascending degrees formatted to 15 and 4 significant digits for the responsivity and uncertainty regression functions, respectively. These coefficients are provided in tabulated form for

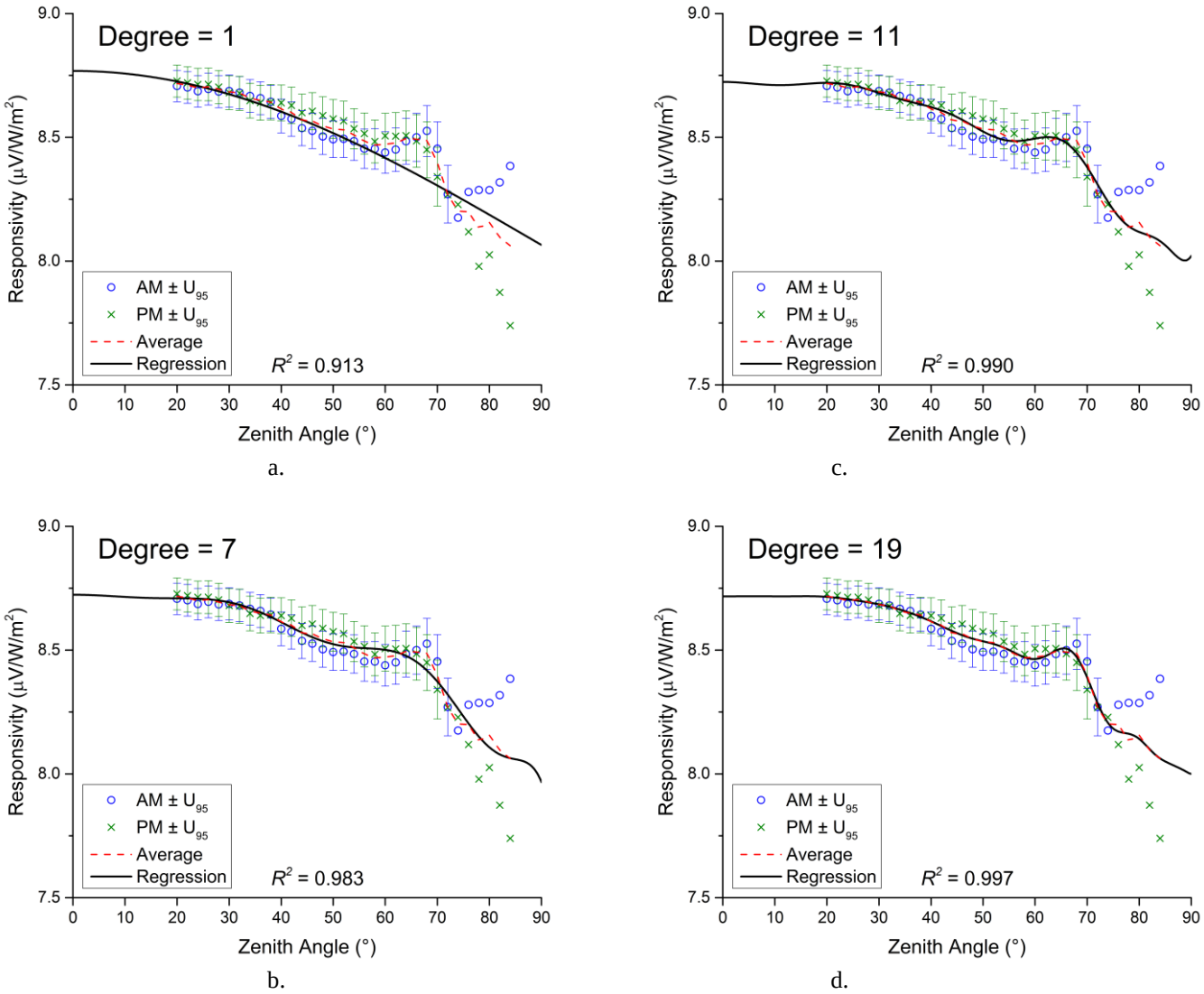

Fig. 9. The polynomial regression fits of the averaged morning (AM) and afternoon (PM) responsivities for an all-black thermopile pyranometer, showing the closer fits of progressively higher degree polynomials. The program parameters for these fits, in order from (a.)-(d.) are: (1,2,1,0), (7,2,1,0), (11,2,1,0), and (19,2,1,0).

implementation in spreadsheet software and in comma-delimited form for implementation in a programming environment.

5. Testing

The software tool was used to evaluate how well the algorithms fit regression functions to calibration data of various pyranometers of multiple models. All data were measured at NREL according to the BORCAL procedure. Calibration data sets from approximately 40 different pyranometers of six (6) different models were fit with regression functions, with all closely fitting the data from adjusting only the program parameters. Results for a black-and-white pyranometer, a diffused silicon cell, and another all-black thermopile pyranometer are shown in the above figures, with the program fit settings given in the captions in the following format: (Degree, Extrap. Order High, Extrap. Order Low, Num. To Ignore High, [Num. To Ignore Low]). The settings for the fits in Fig. 4 and 5 above are (20,2,2,0) and (29,1,2,0,0) for the averaged and separate responsivities, respectively.

The regression fits of the calibration data for a black-and-white pyranometer are shown in Fig. 7. There are significant differences at higher zenith angles between the AM and PM responsivities, and there is a relatively large 3.5 % difference between the AM responsivities at -45° and -70°. The AM and PM responsivities are kept separate to demonstrate the ability of the algorithms to create a complicated yet true fit for use during times when the calibration conditions are confidently duplicated.

The regression fits shown in Fig. 8 are through the averaged AM and PM calibration data from a domed diffused silicon-cell pyranometer. This type of pyranometer exhibits a negative

curvature responsivity curve, opposite of the positive curvature curves more typical of the thermopile pyranometers.

Regression fits of the averaged AM and PM calibration data from an all-black thermopile pyranometer are shown in Fig. 9, each with progressively higher degree fits. The top, first regression fit has a degree of one (1), with an R^2 value of 0.913, and nearly fits within all of the individual data point uncertainties. The next two fits have degrees and R^2 values of 7 and 11, and 0.983 and 0.990, respectively, and these both fit within all of the individual data point uncertainties. The last fit with a degree of 19 and an R^2 value of 0.997 is a near perfect fit to the average of the AM and PM calibrated responsivities, using program parameters (19,2,2,0).

6. Conclusions

The first algorithm presented here creates robust, high precision single polynomial fits of pyranometer responsivities as a function of incidence angle that can be easily implemented in spreadsheet software or programming environments for when the conditions experienced by the pyranometer match those observed during calibration. These functions have no overshoots and minimal oscillations between data points, and include extrapolations to 0° and 90° incidence angles. The second presented algorithm creates conservative, simple regression fits of the responsivity uncertainties as a function of incidence angle that are also easily implemented in software.

Both the responsivity and uncertainty regression algorithms have been employed in a custom software program that can be freely downloaded at http://www.nist.gov/el/building_environment/heattrans/. This software displays both regression fits and outputs their coefficients in two formats for use in either spreadsheet or programming environments. The software code is open source and therefore can be inspected, modified, and compiled for other operating systems.

The regression algorithms were tested using the software program and calibration data from 40 pyranometers of six (6) different models, including all-black thermopile, black and white thermopile, and domed diffused silicon-cell pyranometers. All of the obtained regression functions closely represented the associated data sets with R^2 values greater than 0.98 for the responsivity fits. The responsivity function values were also within all of the individual data point uncertainty bounds when a high degree fit was selected.

7. Future Research

Follow-up research will be performed to investigate the impact of using these incidence angle dependent pyranometer responsivities on the accuracy of the measurements for various types of pyranometers, including thermopile and silicon cell types. It has yet to be shown how the accuracy of pyranometers is affected over the long-term when using incidence angle dependent responsivities and what impact it will have during cloudy and variable sky conditions when the beam radiation at its associated incidence angle is not the dominant solar component.

Acknowledgements

The author gratefully acknowledges the feedback and expert guidance of NREL senior scientists Ibrahim Reda and Afshin Andreas and ASTM Subcommittee G03.09 on Radiometry chairman Daryl Myers.

References

ASTM/G03 Committee, 2010. Standard Test Method for Calibration of a Pyranometer Using a Pyrheliometer (Standard No. G167-05(2010)). ASTM International.

Fritsch, F. N., Carlson, R.E., 1980. Monotone Piecewise Cubic Interpolation. SIAM J. Numerical Analysis, 17, 238-246.

Granata, J., Howard, J., 2011. PV validation and bankability workshop: San Jose, California (No. DOE/GO-102011-3476). Energy Efficiency & Renewable Energy (EERE).

IEEE, 2008. IEEE Standard for Floating-Point Arithmetic (Standard No. 754-2008).

JCGM/WG 1, 2010. Evaluation of measurement data - Guide to the expression of uncertainty in measurement (100:2008). Working Group 1 of the Joint Committee for Guides in Metrology.

Kahaner, D., Moler, D., Nash S., 1988. Numerical Methods and Software. Prentice Hall.

Lane, T. P., DuMouchel, W.H., 1994. Simultaneous Confidence Intervals in Multiple Regression. The American Statistician 48, 315–321.

Lester, A., Myers, D.R., 2006. A method for improving global pyranometer measurements by modeling responsivity functions. Solar Energy 80, 322–331.

MATLAB, 2010. The Mathworks Inc., Natick, MA.

Meeus, J., 1998. Astronomical Algorithms, Second edition. Willmann-Bell, Inc., Richmond, VA.

Michalsky, J.J., 1988. The Astronomical Almanac's Algorithm for Approximate Solar Position (1950-2050). Solar Energy 40, 227-235.

Michalsky, J.J., et al., 2005. Toward the development of a diffuse horizontal shortwave irradiance working standard. Journal of Geophysical Research: Atmospheres 110, D06107.

Myers, D.R., Stoffel, T.L., Reda, I., Wilcox, S.M., Andreas, A.M., 2002. Recent Progress in Reducing the Uncertainty in and Improving Pyranometer Calibrations. Journal of Solar Energy Engineering 124, 44–50.

Reda, I., 1998. Improving the accuracy of using pyranometers to measure the clear sky global solar irradiance (No. NREL/TP-560-24833).

Reda, I., Myers, D., Stoffel, T., 2008. Uncertainty estimate for the outdoor calibration of solar pyranometers: a metrologist perspective. NCSLI Measure 3, 58–66.

Seber, G. A. F., Wild, C. J., 2003. Nonlinear Regression. Wiley-Interscience, Hoboken, NJ.

Taylor, B.N., Kuyatt, C.E., 2004. Guidelines for Evaluating and Expressing the Uncertainty of NIST Measurement Results (NIST Technical Note No. 1297). National Institute of Standards and Technology.